

# Homo- and hetero-epitaxial growth of hexagonal and cubic $\text{Mg}_x\text{Zn}_{1-x}\text{O}$ alloy thin films by pulsed laser deposition technique

S S Hullavarad<sup>1,4</sup>, N V Hullavarad<sup>1</sup>, D E Pugel<sup>2,5</sup>, S Dhar<sup>2</sup>,  
I Takeuchi<sup>2</sup>, T Venkatesan<sup>2</sup> and R D Vispute<sup>3</sup>

<sup>1</sup> Office of Electronic Miniaturization, University of Alaska Fairbanks, Fairbanks, AK 99701, USA

<sup>2</sup> Center for Superconductivity Research, Department of Physics, University of Maryland, College Park, MD 20742, USA

<sup>3</sup> Blue Wave Semiconductors, Columbia, MD, USA

E-mail: [fnssh1@uaf.edu](mailto:fnssh1@uaf.edu)

Received 21 February 2007, in final form 23 June 2007

Published 3 August 2007

Online at [stacks.iop.org/JPhysD/40/4887](http://stacks.iop.org/JPhysD/40/4887)

## Abstract

In this work, we describe the homo- and hetero-epitaxial growth of hexagonal and cubic  $\text{Mg}_x\text{Zn}_{1-x}\text{O}$  thin films on lattice matched substrates of  $c\text{-Al}_2\text{O}_3$ , ZnO, MgO and  $\text{SrTiO}_3$ . The crystalline quality, composition and epitaxial nature of the alloy films are obtained by x-ray diffraction and Rutherford backscattering spectroscopy (RBS) techniques. The RBS channeling yields are in the range 3–8% for homoepitaxial and hetero-epitaxial thin films. The metal–semiconductor–metal and ultraviolet detectors were fabricated on hexagonal and cubic  $\text{Mg}_x\text{Zn}_{1-x}\text{O}$  thin films and the leakage current and UV-visible rejection ratio are correlated with the epitaxial relationship between the film and substrates.

(Some figures in this article are in colour only in the electronic version)

## 1. Introduction

For the first time, ZnO thin films were grown by the sputtering technique on sapphire substrates (hexagonal structure as that of ZnO and excellent thermal conductivity) in 1966 by Rozgonyi and Pouto [1, 2]. Reactive sputtering and chemical vapour transport techniques dominated the ZnO thin film research arena for almost a decade to understand the optical [3–5], especially surface acoustic properties [6–8]. ZnO now finds application in phosphors, paints, piezoelectric transducers, varistors and transparent conducting films, the latter being important for the photovoltaic industry. More details on the ZnO growth techniques, devices and issues are discussed in a comprehensive review elsewhere [9]. The trend continued

until the early 1990s when the GaN technology started showing hopes of blue LED/lasers and crystal growth research took another turn in achieving high quality single crystals [10]. The curiosity to explore the wide band gap materials to achieve blue and UV light emission and detection from solid-state junctions paved the way for the discovery of blue light emitting diode and many discoveries to fine tune the device properties using different growth techniques and engineering novel device structures. It was well known throughout that the epitaxial nature of the films played a vital role in controlling the opto electronic properties. So major emphasis was laid on understanding and identifying lattice matched substrates in order to achieve defect free (threading dislocations due to interface related defects) device quality material. The major drawback with GaN and its related alloys of AlGaIn is its failure under radiation environment as shown by Legodi *et al* [11]. The authors have studied high energy proton and

<sup>4</sup> Author to whom any correspondence should be addressed.

<sup>5</sup> NASA Goddard Space Flight Center, Detector Systems Branch, Greenbelt, MD 20742, USA.

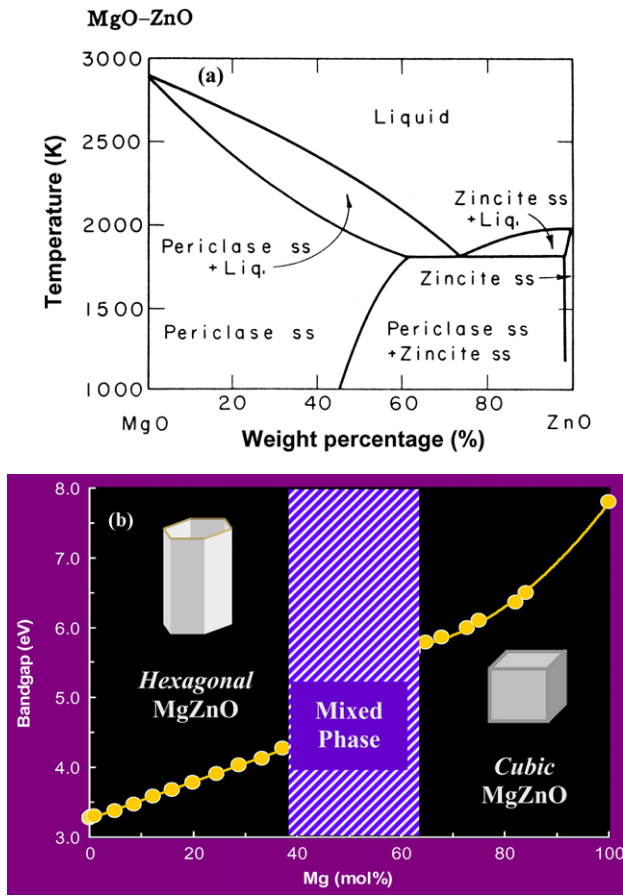


**Figure 1.** (a) Phase diagram of an MgO-ZnO alloy. The solid solubility of MgO in ZnO is only 2 wt% at thermal equilibrium. Note the limited solubility of Mg in ZnO [14]. (b) Phase diagram of (energy gap versus MgO composition) Mg<sub>x</sub>Zn<sub>1-x</sub>O alloy thin films as a function of the Mg content in ZnO from [15].

helium irradiation effects on the Al<sub>x</sub>Ga<sub>1-x</sub>N metal/Schottky-type structure photodetector diodes with cut-off wavelengths of 250 and 300 nm, corresponding to Al mole fractions  $x = 0.41$  and  $0.12$ . ZnO is shown to have better radiation hardness as compared with many other wide band gap optoelectronic materials [12]. Sapphire substrate despite its poor structural mismatch with ZnO and GaN has been an inevitable choice due to its low cost, availability in large area wafers and a wide band gap. However, the performance of optoelectronic devices, in particular, light emission, depends on the density of dislocations arising mostly due to the lattice mismatch between the substrate and the film. Detchprohm *et al* [13] demonstrated the use of ZnO buffer layers to grow epitaxial GaN thick films on sapphire paving the way for homoepitaxy in wide bandgap optoelectronics research and applications (lattice mismatch between GaN and ZnO—1.8%).

Another important semiconductor alloy that is analogous to AlGaN is magnesium zinc oxide (MgZnO) which is realized by alloying ZnO with MgO. MgO as such in the bulk form has a solid solubility limit of 2 wt% in ZnO [14] as shown in figure 1(a). In the thin film form, MgO is completely miscible in ZnO. We have reported the complete band gap alloying of Mg<sub>x</sub>Zn<sub>1-x</sub>O for the Mg composition in the range  $x = 0-1$  on sapphire substrates using the pulsed laser deposition (PLD)

technique [15]. As shown in figure 1(b), the Mg<sub>x</sub>Zn<sub>1-x</sub>O thin films with Mg composition  $0 < x < 0.37$  have a hexagonal wurtzite crystal structure (h-MgZnO). Without the phase separation, the maximum achievable band gap for hexagonal Mg<sub>x</sub>Zn<sub>1-x</sub>O is 4.28 eV. Further increase of Mg in Mg<sub>x</sub>Zn<sub>1-x</sub>O alloy leads to a mixed region of hexagonal and cubic phases with undefined energy band gaps. When the Mg composition exceeds 62%, the cubic(c-MgZnO) phase starts forming ( $0.62 < x < 1$ ). The band gap of c-MgZnO varies from ~5.4 to 7.8 eV, depending upon the Zn/Mg content in the film, thus extending the detection of complete UV spectrum possible in all three regions UV-A (320–400 nm) to UV-B (280–320 nm) and UV-C (200–280 nm). MgZnO is a technologically important semiconductor material [16], which potentially has wide applications in wireless communications, optoelectronics [17], including ultraviolet diode lasers and sensors [18] and MEMS technology. This material is of significant importance for various applications in flame sensors, UV index monitors and missile plume detection.

In the present work, we have used the PLD technique to deposit MgZnO thin films. The inherent nature of non-thermal equilibrium condition achieved during the PLD process enables the solubility of these alloys. In the past, there have been reports of the solid solubility of MgO in ZnO to be 33% for thin film alloys under metastable conditions [19]. While studying the optimization conditions, we found that the solubility of MgO in ZnO films is a function of growth temperature and this factor is critical for stabilizing the structure and the chemical phase purity of the alloys. Sharma *et al* studied the optical and structural properties of PLD Mg<sub>x</sub>Zn<sub>1-x</sub>O thin films for a Mg concentration up to 33% [20]. The room temperature broadening of optical emission, absorption coefficient, exciton binding energy gaps and binding energies of PLD Mg<sub>x</sub>Zn<sub>1-x</sub>O up to  $x = 36$  thin film alloys on sapphire substrates were studied by transmission spectroscopy [21]. The single phase, metastable wide band gap (5–6 eV) PLD grown epitaxial Mg<sub>x</sub>Zn<sub>1-x</sub>O thin films on sapphire for a Mg composition of 50% were reported and the authors noted that the composition, the structure and the band gaps of alloy thin films depend critically on the growth temperature [22]. Lorenz *et al* [23] have studied the electrical doping of ZnO by Ga and Al and band gap alloying with Mg and Cd. They employed the PLD technique to grow doped and alloy thin films on c-sapphire substrates and Hall measurements to monitor the carrier concentration of the films. Apart from measuring the band gap of resulting alloys, the authors noted the variation in the carrier concentration of the thin films to the tune of 6 orders and high mobility in heteroepitaxial layers.

It is generally accepted that PLD is capable of providing epitaxial thin films under optimized conditions [24]. However, one needs to control the particulate density, which is a common problem, termed as splashing in PLD [25]. Splashing occurs due to one of the following reasons [26]: (1) subsurface boiling, (2) expulsion of the liquid layer by the shock wave pressure and (3) exfoliation. The laser ablated material consists of macroscopic droplets of size 1–10 μm diameter. The ablated particles ride on the shock wave over a short period of distance by laser impact on the target and then diffuse through the ambient (reactive gas, usually O<sub>2</sub>, N<sub>2</sub>, Ar + H<sub>2</sub>, NH<sub>3</sub>, Ar,

He). The elimination of droplets in PLD is an experimental trick that involves optimization of various parameters such as laser energy density, substrate to target distance, background gas pressure, substrate temperature, target preparation, target density and target rotation rate, which are dependent on each other. Reduction of laser energy is regarded as one of the straightforward ways to reduce the particulate density but one has to sacrifice with the crystalline quality and the deposition rate. For example, in the case of deposition of AlN as a capping agent for dopant activation in SiC, the droplets cause severe difficulties in device operation as debris during chemical cleaning after annealing of the AlN/SiC structures [27]. Koinuma *et al* [28], have developed a novel technique, which is a modification of the existing PLD technique termed as the laser MBE technique to improve the overall quality of metal oxide thin films. This method involves monitoring of the thin film growth by *in situ* reflection high energy electron diffraction set-up.

Several deposition techniques used to deposit MgZnO thin films such as, plasma assisted MBE [29, 30], electron beam evaporation [31], hybrid technique involving MOCVD and reactive sputtering [32], low temperature physical deposition [33] and co-evaporation [49] have been reported. There have been reports on theoretical studies in ZnO/MgZnO quantum well heterostructures—excitonic transition energies (assuming exciton–phonon interaction) [34, 35] and electronic structures by empirical pseudo-potential method [36]. On the devices front based on MgZnO alloys, p–n junction LEDs fabricated from MgZnO/ZnO/AlGaIn/GaN triple heterostructures with the turn-on voltage of 3.2 V and light emission at 390 nm [37], MIS structures with a current density of  $1 \times 10^{-7} \text{ A cm}^{-2}$  at  $700 \text{ kV cm}^{-1}$  [38], have been demonstrated. The optical properties of MgZnO nanomaterials have been studied [39] using PL and Raman spectroscopy measurements [40] and are also employed as linkers with acidic groups to study the effect of pH pretreatment of the surface binding [41].

Most of the ZnO and MgZnO alloy thin films have been deposited on basal plane (0001) sapphire substrates, which have 17% lattice mismatch with respect to ZnO. All these deposited ZnO and MgZnO samples and heterostructures feature the polar (0001) orientation (either O or Zn terminated), and hence they exhibit strong polarization and piezoelectric fields [42]. These polarization fields give rise to significant lattice strains and increase the interface strain-related defects that in turn affect the device properties. To avoid such effects, in the past, R-plane sapphire substrates have been used to deposit ZnO and its alloys [43]. The effect of lattice matching on the optical properties of ZnO quantum well superlattices with higher band gap alloys was very well demonstrated by Makino *et al* [44]. Coupled with mismatches in thermal expansion coefficients, the misfit dislocations produced in the films during the heteroepitaxial growth pose a limitation to the ultimate performance of oxide based UV detectors and light emitters. For optoelectronic device applications it is imperative that these films have to be grown on lattice matched substrates [45] to reduce the interface dislocation density as the quantum efficiency of many optoelectronic devices depends on the defect densities [46]. It is thus important to study the effect of substrate (lattice structures, orientation, lattice constants and surface chemistry) on the growth dynamics of thin films.

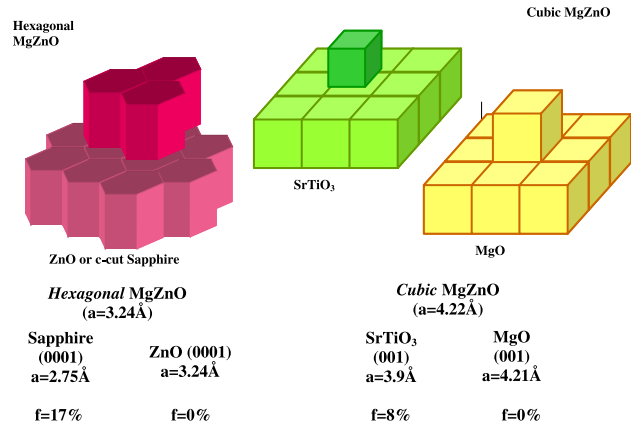


**Figure 2.** Schematic of homo- and hetero-epitaxy of  $\text{Mg}_{0.15}\text{Zn}_{0.85}\text{O}$  (hexagonal) on ZnO and c- $\text{Al}_2\text{O}_3$  and  $\text{Mg}_{0.9}\text{Zn}_{0.1}\text{O}$  (cubic) alloy thin films on  $\text{SrTiO}_3$  and MgO substrates. The lattice misfit parameter  $f$  is defined as  $f = (a_{\text{film}} - a_{\text{substrate}}) / a_{\text{substrate}}$  and expressed as a percentage [62].

In this work, we describe the method to improve the device response of metal–semiconductor–metal (MSM) devices formed on hexagonal and cubic films (homo- and heteroepitaxial) grown on lattice matched substrates. The substrates are chosen in such a way that they match the lattice structure of  $\text{Mg}_x\text{Zn}_{1-x}\text{O}$  for hexagonal and cubic phases. Figure 2 shows the schematic of homo- and heteroepitaxy of  $\text{Mg}_x\text{Zn}_{1-x}\text{O}$  alloys on ZnO and c- $\text{Al}_2\text{O}_3$  substrates for hexagonal alloys and  $\text{SrTiO}_3$  and MgO substrates for cubic alloys. The hexagonal alloys have a lattice matching of 0% and 17% and cubic alloys have a lattice mismatch of 8% and 0% respectively, with reference to the corresponding substrates. In this study, hexagonal alloys corresponding to the Mg composition of 15% and cubic alloys corresponding to the Mg composition of 90% are chosen because the hexagonal and cubic structure films of these compositions match the selected substrates closely than the higher Mg (>15–32%) for hexagonal and the lower Mg (<90%) for cubic phases on respective substrates.

## 2. Experimental

Thin films of  $\text{Mg}_x\text{Zn}_{1-x}\text{O}$  alloys were fabricated on single crystal ZnO (O surface terminated Cermet), c-plane (0001) sapphire ( $\text{Al}_2\text{O}_3$ ),  $\text{SrTiO}_3$  and MgO substrates by the PLD technique. The substrates were cleaned by ordinary propanol, acetone and methanol solutions in ultrasonic bath for 2 min individually without any acidic treatment because acidic media preferentially etch away the ZnO substrate in particular and introduces roughness in general on all substrates. However, substrates were thermally treated in vacuum for 30 min prior to deposition. The target was mounted in a high vacuum chamber with a base pressure of  $1 \times 10^{-7}$  Torr. Due to higher vapour pressure of Zn than Mg, the composition of  $\text{Mg}_x\text{Zn}_{1-x}\text{O}$  films deviated significantly from that of the target. In our previous work [15], we have shown that for a given Mg composition in the MgZnO target, the composition in the film varies as a function of deposition temperature. For example, an Mg composition of 68% in the MgZnO target results in 40% of MgZnO films when deposited at room temperature, 70%

when deposited at 400 °C and 85% when deposited at 800 °C. The composition is obtained by Rutherford backscattering spectroscopy (RBS) and energy dispersive spectrometry (EDS) techniques. We have observed in our optimization experiments that the smoothness and the stoichiometry of thin films depend on the density of the targets. The desired quantities of MgO and ZnO powders were first weighed. The powder mixture was ball milled for 24 h and then sintered for 800 °C for 12 h in oxygen atmosphere. The sintered mixture was again crushed to fine powders and palletized to 1 in. diameter and then finally sintered to 1100 °C for 12 h in oxygen atmosphere. The partial oxygen pressure ( $1 \times 10^{-4}$  Torr) and the substrate temperature (750 °C) were optimized for better crystalline and optical properties of thin films. The KrF excimer laser pulses (248 nm, 10 Hz,  $\sim 1.7 \text{ J cm}^{-2}$ ) were focused on an MgZnO alloy target creating a plasma plume depositing a smooth thin film on the substrate held at 15 cm from the target with a deposition rate of  $0.3 \text{ \AA/pulse}$ . The deposition was carried out for 45 min to obtain films of thickness  $\sim 5000\text{--}7000 \text{ \AA}$ .

The crystalline quality of the films was examined using four-circle x-ray diffraction (XRD) using the Siemens D 5000 Diffractometer. The quantitative analysis of the crystalline quality and the nature of interface between the film and substrate was carried out by RBS and ion channelling techniques using a well-collimated beam of 1.5 MeV  $\text{He}^+$  ions. The ratio of the (RBS yield— $\chi_{\text{min}}$ ) with the incident beam along (channelled) that of a random direction, respectively, provides information on the crystalline quality of the film. The film thickness was determined using a computer fitting program, in which the thickness is iteratively adjusted until the theoretical curve matched the experimental plot. It should be noted that there always exist dislocations close to the interface due to a large lattice mismatch between the film and the substrate.

To study the effect of epitaxial growth on the electrical transport and the photoresponse measurements, the UV detectors were fabricated on homo- and heteroepitaxially grown  $\text{Mg}_x\text{Zn}_{1-x}\text{O}$  films, in MSM configuration with interdigitized electrodes. The interdigital metal electrodes, which were defined on a 150 nm thick Cr/Au bilayer by conventional photolithography, are 250  $\mu\text{m}$  long, 5  $\mu\text{m}$  wide and have an interelectrode spacing of 5  $\mu\text{m}$ . To insure Ohmic contact, a thin adhesion layer of chromium was used. A continuous light output from a Xe (300 W) arc lamp passing through a Thermo Oriel monochromator (1200 lines  $\text{mm}^{-1}$  grating with optical chopper) was incident on the UV detectors. The incident light of wavelengths 310 and 170 nm corresponding to bandgaps that were derived from the UV absorption edges for hexagonal and cubic alloys was selected from the independent UV-Visible transmission spectroscopy measurements. The incident light power was calibrated for both wavelengths considering the variation of power with the wavelength of the incident light.

### 3. Results and discussion

Figures 3(a) and (b) and 4(a) and (b) show the XRD  $\theta$ - $2\theta$  and rocking curve scans for the  $\text{h-Mg}_{0.15}\text{Zn}_{0.85}\text{O}$  (hexagonal) films grown on single crystal ZnO and  $\text{Al}_2\text{O}_3$  substrates, respectively. The XRD peak positions and phase identification have been adopted from the work by

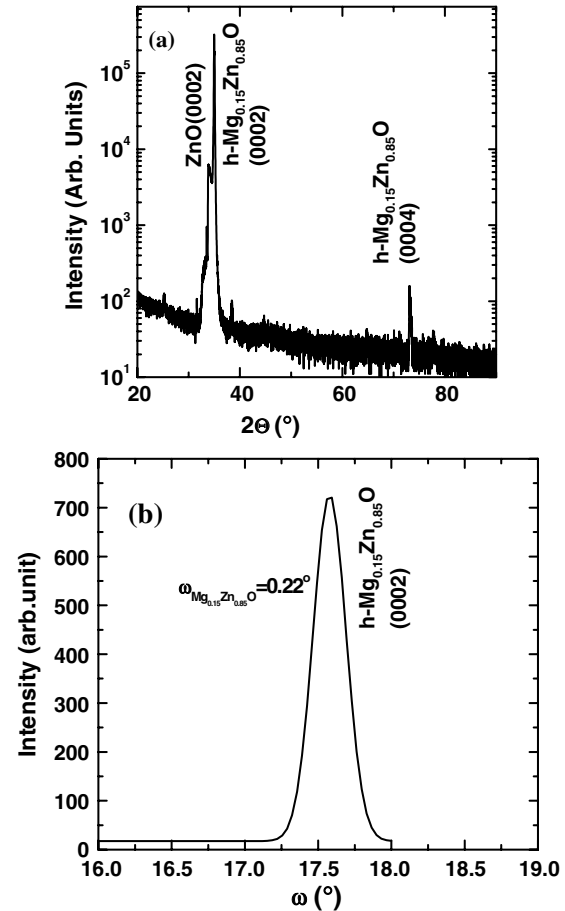


**Figure 3.** XRD (a)  $\theta$ - $2\theta$  and (b) rocking curve scans for the  $\text{Mg}_{0.15}\text{Zn}_{0.85}\text{O}$  films grown on the single crystal ZnO substrate.

Takeuchi *et al* [47] where the detailed XRD analysis of the combinatorial spread of MgO-ZnO thin films deposited by the PLD technique has been reported. The peaks around  $2\theta = 34.3^\circ$  correspond to (0002) orientation of the MgZnO hexagonal structure [48]. The  $\text{h-Mg}_{0.15}\text{Zn}_{0.85}\text{O}$  films show strong (0002) and (0004) reflections in both cases. The epitaxial relationship of  $(0001)_{\text{h-MgZnO}}/(0001)_{\text{S}}$  between the hexagonal  $\text{Mg}_{0.15}\text{Zn}_{0.85}\text{O}$  and  $\text{Al}_2\text{O}_3$  substrates is quite obvious. The rocking curve full width at half maximum (FWHM) as shown in figures 3(b) and 4(b) is  $0.2^\circ$  and  $0.26^\circ$  for the  $\text{h-Mg}_{0.15}\text{Zn}_{0.85}\text{O}$  films grown on ZnO and  $\text{Al}_2\text{O}_3$ , respectively [49]. It is clearly seen that the slightly wider curve shape for the film grown on  $\text{Al}_2\text{O}_3$  is a consequence of lattice mismatch of around 17%, whereas in the case of  $\text{h-Mg}_{0.15}\text{Zn}_{0.85}\text{O}$  film grown on the ZnO substrate there is a complete substrate to film lattice matching [50]. Due to the large lattice mismatch and the thermal expansion coefficient between the  $\text{h-Mg}_{0.15}\text{Zn}_{0.85}\text{O}$  thin films and the  $\text{Al}_2\text{O}_3$  substrate, thin films tend to grow with biaxial strain. The induced strain manifests in the form of piezoelectric effects, which in turn shortens the carrier lifetime proving detrimental to the operation of optoelectronic devices [51].

Figure 5 shows the aligned and random backscattering spectra for the  $\text{h-Mg}_{0.15}\text{Zn}_{0.85}\text{O}$  film on the  $\text{Al}_2\text{O}_3$  substrate. The minimum channelling yield  $\chi_{\text{min}}$  near the surface region of the film is 7%. The higher channelling yield as compared

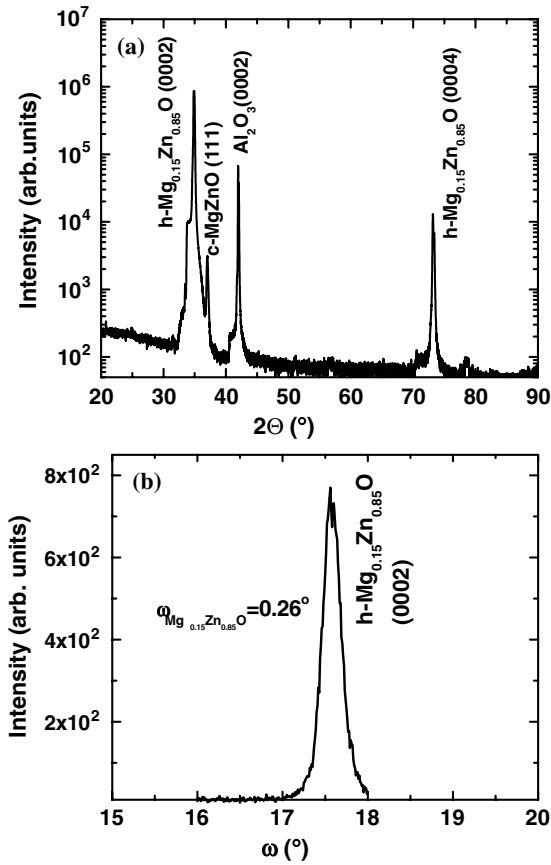


**Figure 4.** XRD (a)  $\theta$ - $2\theta$  and (b) rocking curve scans for the  $\text{Mg}_{0.15}\text{Zn}_{0.85}\text{O}$  films grown on the c- $\text{Al}_2\text{O}_3$  substrate.

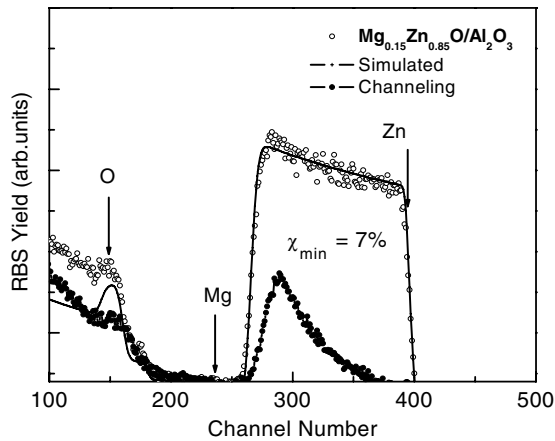


**Figure 5.** RBS spectra of  $\text{Mg}_{0.15}\text{Zn}_{0.85}\text{O}$  thin films grown on the c- $\text{Al}_2\text{O}_3$  substrate. The channelling yield was measured to be 7%.

with ZnO thin film on the  $\text{Al}_2\text{O}_3$  substrate ( $\chi_{\min} = 3\%$  [52]) is attributed to the interface defects between the film and the substrate. Bendersky *et al* [53] have studied the MgO and ZnO composition spread grown by PLD on a single chip by using high resolution cross-sectional transmission electron measurements and noted the planar defects laying predominantly parallel to the interface in regions of h- $\text{Mg}_x\text{Zn}_{1-x}\text{O}$  thin films on  $\text{Al}_2\text{O}_3$  substrates. We have observed that the ZnO single crystal undergoes crystal and surface

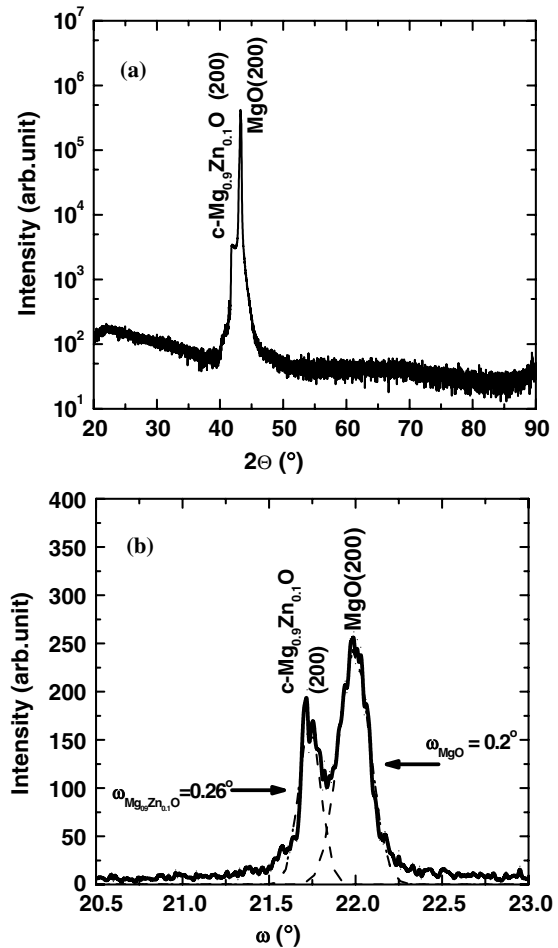


**Figure 6.** XRD (a)  $\theta$ - $2\theta$  and (b) rocking curve scans for the  $\text{Mg}_{0.9}\text{Zn}_{0.1}\text{O}$  films grown on the single crystal MgO substrate.

degradation when annealed to temperatures of 400–500 °C and then regains the crystalline quality after annealing at around 900 °C. Channelling experiments on single crystal ZnO are underway and are time consuming because of the unavailability of good quality substrates on time and the surface inhomogeneities associated with the surface polarity.

Figures 6(a) and (b) show the XRD  $\theta$ - $2\theta$  and rocking curve scans for the c- $\text{Mg}_{0.9}\text{Zn}_{0.1}\text{O}$  (cubic) alloy thin films grown on the single crystal MgO substrate. The peak at  $2\theta = 41.9^\circ$  corresponds to (200) orientation of the  $\text{Mg}_x\text{Zn}_{1-x}\text{O}$  cubic structure. The rocking curve of FWHM as shown in figure 6(b) is  $0.26^\circ$  for the c- $\text{Mg}_{0.9}\text{Zn}_{0.1}\text{O}$  film. Because of the lattice matching of the c- $\text{Mg}_{0.9}\text{Zn}_{0.1}\text{O}$  thin film with the MgO substrate due to higher Mg concentration, the XRD (100) peak reflections corresponding to the substrate appear very close to the film peaks. The rocking curves have been deconvoluted to resolve and quantify the FWHM of the film and the substrate. The rocking curve FWHM values for the c- $\text{Mg}_{0.9}\text{Zn}_{0.1}\text{O}$  film and the MgO substrate are calculated to be  $0.26^\circ$  and  $0.2^\circ$ , respectively. This is obvious as the composition of the  $\text{Mg}_{0.9}\text{Zn}_{0.1}\text{O}$  films is close to the composition of the MgO substrate and reflects on the optimized growth conditions achieved in the present PLD growth technique. The calculated  $a$ -parameter of c- $\text{Mg}_{0.9}\text{Zn}_{0.1}\text{O}$  is  $4.22 \text{ \AA}$ , which is very close to that of MgO ( $a = 4.21 \text{ \AA}$ ) [54].

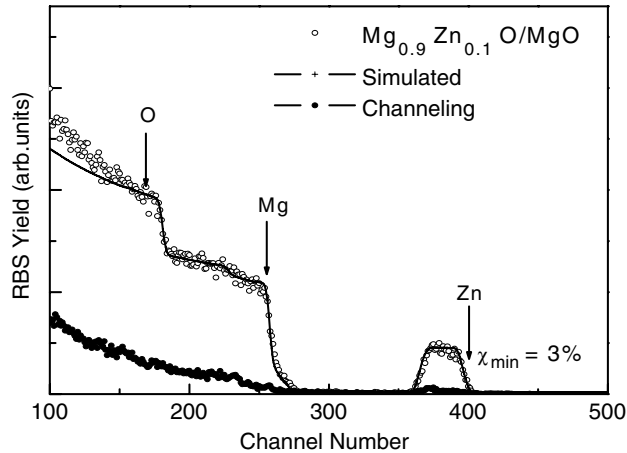


**Figure 7.** RBS spectra of  $\text{Mg}_{0.9}\text{Zn}_{0.1}\text{O}$  thin films grown on the  $\text{MgO}$  substrate. The channelling yield was measured to be 3%.

Figure 7 shows the aligned and random backscattering spectra for the  $c\text{-Mg}_{0.9}\text{Zn}_{0.1}\text{O}$  film on the  $\text{MgO}$  substrate. The minimum channelling yield  $\chi_{\min}$  near the surface region of the films is 3% for  $c\text{-Mg}_{0.9}\text{Zn}_{0.1}\text{O}$  on  $\text{MgO}$ , indicating a high degree of crystallinity. From the figure it is clear that the channelling yield at the surface is very low and provides a quantitative insight into the crystal quality which is very crucial in device fabrication and as a template for growing multilayers.

Figures 8(a) and (b) show the XRD  $\theta$ - $2\theta$  and rocking curve scans for the  $c\text{-Mg}_{0.9}\text{Zn}_{0.1}\text{O}$  cubic alloy thin films grown on the single crystal  $\text{SrTiO}_3$  substrate. The appearance of only the (001) peak indicates that the films are highly  $c$ -axis oriented and corresponds to the cubic structure of  $c\text{-Mg}_{0.9}\text{Zn}_{0.1}\text{O}$ . The peak at  $2\theta = 43.4^\circ$  corresponds to (200) orientation of the  $\text{MgZnO}$  cubic structure. The FWHM for the XRD-rocking curve was about  $0.41^\circ$ . Figure 9 shows the random and aligned RBS spectra of a  $c\text{-Mg}_{0.9}\text{Zn}_{0.1}\text{O}$  film grown on  $\text{SrTiO}_3$  substrates. The channelling yield  $\chi_{\min}$  for these films is found to be 8% under optimized growth conditions.

The optical bandgaps of  $\text{h-Mg}_{0.15}\text{Zn}_{0.85}\text{O}$  and  $c\text{-Mg}_{0.9}\text{Zn}_{0.1}\text{O}$  thin films grown on double side polished  $\text{Al}_2\text{O}_3$  substrates are obtained from UV-visible transmission experiments (not shown) and are 3.6 eV and 6.9 eV, respectively. For studying the photoresponse measurements on the MSM devices, we used optical excitation wavelengths of 310 and 170 nm corresponding to bandgaps of 4 and 7.3 eV slightly higher than the  $\text{MgZnO}$  thin film bandgaps in this study. Figures 10(a)–(d) show the current-voltage characteristics of homo- and heteroepitaxially grown  $\text{Mg}_x\text{Zn}_{1-x}\text{O}$  films with and without UV illumination. Table 1 summarizes the leakage current, ratio of UV to visible (dark) current and the parameters indicating the crystalline quality obtained from XRD and RBS measurements. Hexagonal  $\text{Mg}_{0.15}\text{Zn}_{0.85}\text{O}$  alloys deposited on  $\text{ZnO}$  and  $\text{Al}_2\text{O}_3$  show leakage currents of  $1 \times 10^{-5}$  A and  $1 \times 10^{-7}$  A, respectively. Both films on  $\text{ZnO}$  and  $\text{Al}_2\text{O}_3$  show a similar UV to visible current ratio of  $1.5 \times 10^3$ . The most intriguing fact in this study is that  $\text{h-Mg}_{0.15}\text{Zn}_{0.85}\text{O}$  despite growing on completely lattice matched  $\text{ZnO}$  (0%) substrate has a larger leakage current than the one growing on the lattice mismatched substrate  $\text{Al}_2\text{O}_3$  (17%). The  $\text{ZnO}$  surface is known to have instability

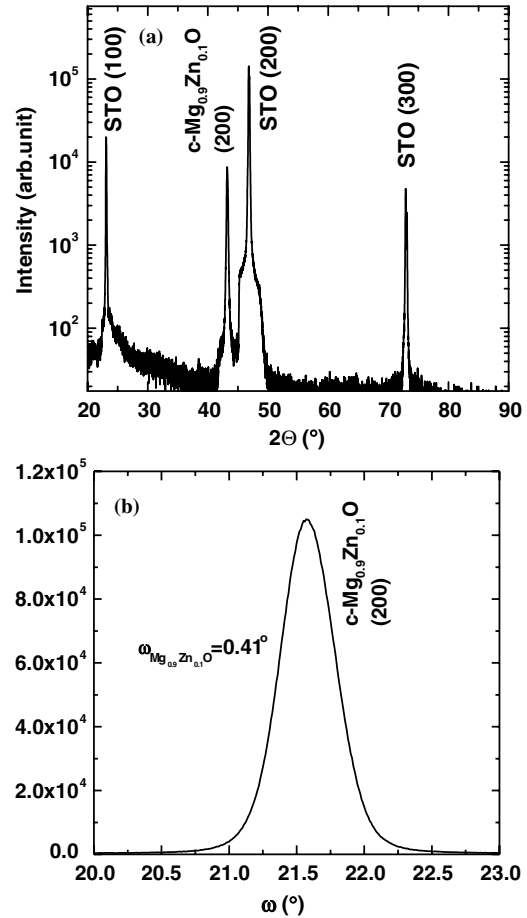


**Figure 8.** XRD (a)  $\theta$ - $2\theta$  and (b) rocking curve scans for the  $\text{Mg}_{0.9}\text{Zn}_{0.1}\text{O}$  films grown on the single crystal  $\text{SrTiO}_3$  substrate.

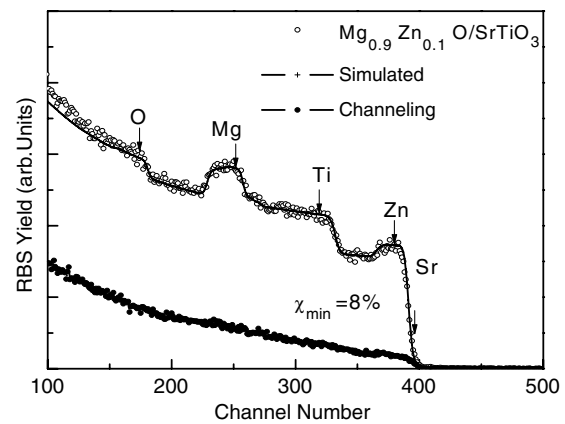


**Figure 9.** RBS spectra of  $\text{Mg}_{0.9}\text{Zn}_{0.1}\text{O}$  thin films grown on the  $\text{SrTiO}_3$  substrate. The channelling yield was measured to be 8%.

due to affinity towards hydroxyl groups, which also varies with the polar surface nature of  $\text{ZnO}$ . Though remarkable progress is made in the development of high quality  $\text{ZnO}$  single crystal substrates by hydrothermal [55], chemical vapour transport [56], and melt growth [57] techniques, there have been reports on the effect of surface instability of  $\text{ZnO}$  single crystals [58]. The  $\text{ZnO}$  single crystal surface exhibits a work function difference between the Zn and the O faces ( $\sim 0.11$  eV). It has also been observed that the surface of

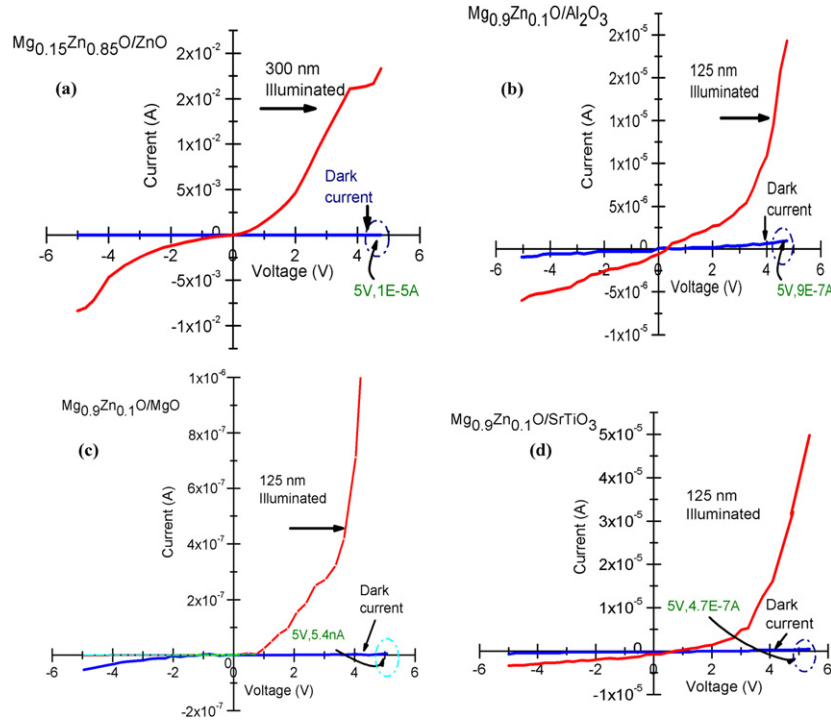


**Figure 10.** Current–voltage characteristics of MSM UV detectors fabricated on (a)  $\text{Mg}_{0.15}\text{Zn}_{0.85}\text{O}/\text{ZnO}$ , (b)  $\text{Mg}_{0.9}\text{Zn}_{0.1}\text{O}/\text{Al}_2\text{O}_3$ , (c)  $\text{Mg}_{0.9}\text{Zn}_{0.1}\text{O}/\text{MgO}$  and (d)  $\text{Mg}_{0.9}\text{Zn}_{0.1}\text{O}/\text{SrTiO}_3$ .

**Table 1.** The dark current at 5 V, UV-dark current ratio for MSM UV detectors fabricated on homo- and heteroepitaxial  $\text{Mg}_x\text{Zn}_{1-x}\text{O}$  thin films on ZnO,  $\text{Al}_2\text{O}_3$ , MgO and  $\text{SrTiO}_3$  substrates. For comparison, the values obtained from XRD and RBS are shown.

$\text{Mg}_x\text{Zn}_{1-x}\text{O}/\text{substrate}$	$I_{\text{dark}}$ at 5 V	$I_{\text{UV}}/I_{\text{dark}}$ at 5 V	XRD $\Delta w$ FWHM( $^\circ$ )	RBS yield (%)
Hex- $\text{Mg}_{0.15}\text{Zn}_{0.85}\text{O}/\text{ZnO}$	$1.0 \times 10^{-5}$	$1.5 \times 10^3$	0.21	NA
Hex- $\text{Mg}_{0.15}\text{Zn}_{0.85}\text{O}/\text{Al}_2\text{O}_3$	$1.0 \times 10^{-7}$	$1.5 \times 10^3$	0.20	7
Cubic- $\text{Mg}_{0.9}\text{Zn}_{0.1}\text{O}/\text{MgO}$	$5.4 \times 10^{-9}$	$1.3 \times 10^3$	0.26	3
Cubic- $\text{Mg}_{0.9}\text{Zn}_{0.1}\text{O}/\text{STO}$	$4.7 \times 10^{-7}$	$1.0 \times 10^2$	0.41	8
Cubic- $\text{Mg}_{0.9}\text{Zn}_{0.1}\text{O}/\text{Al}_2\text{O}_3$	$9.0 \times 10^{-7}$	$2.5 \times 10^1$	0.41	14

ZnO single crystal is unstable at elevated temperatures [59] and undergoes major changes when subjected to different temperature cycles under different gas ambients giving rise to interface-related defects that affect the transport properties. Due to surface inhomogeneities, the homo- or heteroepitaxially growing layer on the ZnO single crystal may find both surfaces with different work functions [60]. However, the surface of  $\text{Al}_2\text{O}_3$  is relatively stable at processing temperatures of at least  $1300^\circ\text{C}$  [61]. The devices fabricated on c- $\text{Mg}_{0.9}\text{Zn}_{0.1}\text{O}$  films grown on MgO,  $\text{SrTiO}_3$  and  $\text{Al}_2\text{O}_3$  (for comparison) have leakage currents of  $5.4 \times 10^{-9}$  A,  $4.7 \times 10^{-7}$  A and  $9 \times 10^{-7}$  A and the ratios of UV to visible currents of  $1.3 \times 10^3$ ,  $1.0 \times 10^2$  and  $2.5 \times 10^1$ , respectively.

The c- $\text{Mg}_{0.9}\text{Zn}_{0.1}\text{O}$  films grown on c- $\text{Al}_2\text{O}_3$  (0002) substrates however were polycrystalline in nature with poor channelling yields due to a large lattice mismatch. The reduced leakage current in the c- $\text{Mg}_{0.9}\text{Zn}_{0.1}\text{O}$  films on MgO is mainly due the reduced lattice strains because of close lattice matching and the stable nature of MgO surface than the surface of ZnO. The upward increase in the leakage current in same alloy composition films on  $\text{SrTiO}_3$  is a consequence of increased lattice mismatch with the substrate. However, the dark current in the case of h- $\text{Mg}_{0.15}\text{Zn}_{0.85}\text{O}$  films on  $\text{Al}_2\text{O}_3$  is  $1 \times 10^{-7}$  A,

as compared with  $9 \times 10^{-7}$  A for c- $\text{Mg}_{0.9}\text{Zn}_{0.1}\text{O}$  on  $\text{Al}_2\text{O}_3$ , with a UV to visible current ratio of 25. It is clear that the interfacial strain induced due to a large lattice mismatch between the c- $\text{Mg}_{0.9}\text{Zn}_{0.1}\text{O}$  thin film and the  $\text{Al}_2\text{O}_3$  substrate as seen from the higher channelling yields, which is a complete heteroepitaxial situation with the cubic film growing on the hexagonal substrate, leads to a poor UV/visible current ratio.

#### 4. Conclusion

In conclusion, we have grown homo- and heteroepitaxial h- $\text{Mg}_{0.15}\text{Zn}_{0.85}\text{O}$  on ZnO and  $\text{Al}_2\text{O}_3$  and c- $\text{Mg}_{0.9}\text{Zn}_{0.1}\text{O}$  films on MgO and  $\text{SrTiO}_3$  substrates. The films show excellent channelling yields from 3% to 8% for the homo- and the heteroepitaxial conditions. The electrical and photo-induced measurements on the devices fabricated on these films provide a clear understanding about the substrate induced effects on the films. The UV to visible current ratios varied from 3 orders of magnitude in homoepitaxially grown films to 1 order for hetero epitaxial films. This study paves the way for the realization of detector improvement methodology for deep UV sensors and provides insight into the understanding of transport properties and individual composition vis-à-vis the crystalline

quality. Due to the lattice matching epitaxy and thermal and optical compatibility between the hexagonal MgZnO film and the ZnO substrate and the cubic MgZnO film and the MgO and SrTiO<sub>3</sub> substrates, the lattice matched heterostructures of h-Mg<sub>0.15</sub>Zn<sub>0.85</sub>O/ZnO and c-Mg<sub>0.9</sub>Zn<sub>0.1</sub>O/MgO may be useful for fabrication of hybrid optoelectronic devices, in particular, light emitting diodes.

## Acknowledgments

The authors gratefully acknowledge the financial support of the National Science Foundation SBIR under Grant No DMI-0321465 and Bluewave Semiconductors, Inc. This work was carried out at the Center for Superconductivity Research, University of Maryland, College Park, USA. The Rutherford backscattering-channelling work reported here was done using the Pelletron shared experimental facility (SEF) supported under the NSF-MRSEC Grant No DMR-00-80008. The authors (SSH and NVH) acknowledge the constant support and encouragement of Professor P C Karulkar, Director and President's Professor, Office of Electronic Miniaturization, and the financial support of the US Defense Micro Electronic Activity (DMEA), US Defense Advanced Research Projects Agency (DARPA) at the University of Alaska Fairbanks.

## References

- [1] Rozgonyi G A and Polito W J 1966 *Appl. Phys. Lett.* **8** 220
- [2] Rozgonyi G A and Polito W J 1969 *J. Vac. Sci. Technol.* **6** 115
- [3] Belt R F and Florio G C 1968 *J. Appl. Phys.* **39** 5215  
Shiosaki T, Ohnishi S, Hirokawa Y and Kawabata A 1978 *Appl. Phys. Lett.* **33** 406
- [4] Galli G and Coker J E 1970 *Appl. Phys. Lett.* **16** 439
- [5] Dybwad G L 1971 *J. Appl. Phys.* **42** 5192
- [6] Vuillod J 1972 *J. Vac. Sci. Technol.* **9** 87
- [7] Ohji K, Yamazaki O, Wasa K and Hayakawa S 1978 *J. Vac. Sci. Technol.* **15** 1601
- [8] Shiosaki T, Ohnishi S, Hirokawa Y and Kawabata A 1978 *Appl. Phys. Lett.* **33** 406
- [9] Ozgur U, Alivov Y I, Liu C, Teke A, Reshchikov M A, Do S, Doan S, Avrutin V, Cho S-J and Morkoc H 2005 *J. Appl. Phys.* **98** 041301
- [10] Nakamura S and Fasol G 1997 *The Blue Laser Diode* (Berlin: Springer)
- [11] Legodi M J, Hullavarad S S, Goodman S A, Hayes M and Auret F D 2001 *Physica B* **308–310** 1189
- [12] Look D C 2001 *Mater. Sci. Eng. B* **80** 383
- [13] Detchprohm T, Amano H, Hiramatsu K and Akasaki I 1993 *J. Cryst. Growth* **128** 384
- [14] West A R 1984 *Solid State Chemistry and its Applications* (Chichester: Wiley)
- [15] Yang W, Hullavarad S S, Nagaraj B, Takeuchi I, Sharma R P, Venkatesan T, Vispute R D and Shen H 2003 *Appl. Phys. Lett.* **82** 3424
- [16] Chen N B and Sui C H 2006 *Mat. Sci. Eng. B* **126** 16
- [17] Tsukazaki A, Ohtomo A, Kawasaki M, Makino T, Chia C H, Segawa Y and Koinuma H 2004 *Appl. Phys. Lett.* **84** 3858
- [18] Hullavarad S S, Dhar S, Varughese B, Takeuchi I, Venkatesan T and Vispute R D 2005 *J. Vac. Sci. Technol. A* **23** 982
- [19] Ohtomo A, Kawasaki M, Koida T, Masubuchi K, Koinuma H, Sakurai Y, Tshida Y, Yasuda T and Sagawa Y 1998 *Appl. Phys. Lett.* **72** 2466
- [20] Sharma A K, Narayan J, Muth J F, Teng C W, Jin C, Kvit A, Kolbas R M and Holland O W 1999 *Appl. Phys. Lett.* **75** 3327
- [21] Teng C W, Muth J F, Ozgur U, Bergmann M J, Everitt H O, Sharma A K, Jin C and Narayan J 2000 *Appl. Phys. Lett.* **76** 979
- [22] Choopun S, Vispute R D, Yang W, Sharma R P, Venkatesan T and Shen H 2002 *Appl. Phys. Lett.* **80** 1529
- [23] Lorenz M *et al* 2003 *Solid State Electron.* **47** 2205
- [24] Jin C M and Narayan R J 2006 *J. Electron. Mater.* **35** 869
- [25] He Y N, Zhang J W, Yang X D, Xu Q A, Liu X H, Zhu C C and Hou X 2005 *Microelectron. J.* **36** 125
- [26] Chrisey D B and Hubler G K 1994 *Pulsed Laser Deposition of Thin Films* (New York: Wiley – Interscience)
- [27] Hullavarad S S *et al* 2006 *J. Electron. Mater.* **35** 777
- [28] Koinuma H, Kawasaki M, Itoh T, Ohtomo A, Murakami M, Jin Z and Matsumoto Y 2000 *Physica C: Superconductivity* **335** 245 and references therein
- [29] Harada C, Ko H J, Makino H and Yao T 2003 *Mater. Sci. Semicond. Proc.* **6** 539
- [30] Wu C X, Lu Y M, Shen D Z, Zhang Z Z, Wei Z P, Zheng Z H, Zhang J Y, Liu Y C and Fan X W 2007 *J. Lumin.* **122** 405
- [31] Chen J, Shen W Z, Chen N B, Qiu D J and Wu H Z 2003 *J. Phys.: Condens. Matter* **15** L475
- [32] Saraf G, Chen Y, Siegrist T, Wielunski L S and Lu Y C 2006 *J. Electron. Mater.* **35** 1306
- [33] Chen N B, Wu H Z, Xu T N and Yu P 2006 *J. Inorg. Mater.* **21** 993
- [34] Coli G and Bajaj K K 2001 *Appl. Phys. Lett.* **78** 2861
- [35] Kang *et al* 2000 *Solid State Commun.* **115** 127
- [36] Fan W J, Xia J B, Agus P A, Tan S T, Yu S F and Sun X W 2006 *J. Appl. Phys.* **99** 013702
- [37] Osinsky A, Dong J W, Kausar M Z, Hertog B, Dabiran A M, Chow P P, Pearton S J, Lopatiuk O and Chernyak L 2004 *Appl. Phys. Lett.* **85** 4272
- [38] Liang J, Wu H Z, Lao Y F, Qiu D J, Chen N B and Xu T N 2004 *Chin. Phys. Lett.* **21** 1135
- [39] Huso J, Morrison J L, Hoeck H, Chen X B, Bergman L, Jokela S J, McCluskey M D and Zheleva T 2006 *Appl. Phys. Lett.* **89** 17
- [40] Bergman L, Morrison J L, Chen X B, Huso J and Hoeck H 2006 *Appl. Phys. Lett.* **88** 2
- [41] Taratula O, Galoppini E, Wang D, Chu D, Zhang Z, Chen H H, Saraf G and Lu Y C 2006 *J. Phys. Chem. B* **110** 6506
- [42] Bernardini F, Feorentini V and Vanderbilt D 1997 *Phys. Rev. B* **56** 10024
- [43] Muthukumar S, Zhong J, Lu Y and Siegrist T 2003 *Appl. Phys. Lett.* **82** 742
- [44] Makino T, Chia C H, Tuan N T, Sun H D, Segawa Y, Kawasaki M, Ohtomo A, Tamura K and Koinuma H 2000 *Appl. Phys. Lett.* **77** 975
- [45] Matsui H and Tabata H 2007 *Phys. Status Solidi c* **3** 4106
- [46] Ohtomo A and Tsukazaki A 2005 *Semicond. Sci. Technol.* **20** S1–12
- [47] Takeuchi I 2003 *J. Appl. Phys.* **94** 7336
- [48] Tanaka H, Fujita S and Fujita S 2005 *Appl. Phys. Lett.* **86** 192911
- [49] Ma J G, Liu Y C, Shao C L, Zhang J Y, Lu Y M, Shen D Z and Fan X W 2005 *Phys. Rev. B* **71** 125430
- [50] Spemann D, Kaidashev E M, Lorenz M, Vogt J and Butz T 2004 *Nucl. Instrum. Methods Phys. Res. B: Beam Interact. Mater. At.* **219** 891
- [51] Makino T, Yasuda T, Segawa Y, Ohtomo A, Tamura K, Kawasaki M and Koinuma H 2001 *Appl. Phys. Lett.* **79** 1282
- [52] Dhar S, Pugel D E, Hullavarad S S, Vispute R D, Ogale S B and Venkatesan T 2006 A two-step process to grow homo-epitaxial ZnO thin film by pulsed laser deposition *J. Electron. Mater.* submitted
- [53] Bendersky L A, Takeuchi I, Chang K-S, Yang W, Hullavarad S and Vispute R D 2005 *J. Appl. Phys.* **98** 083526
- [54] Vashaei Z, Minegishi T, Suzuki H, Hanada T, Cho M W, Yao T and Setiawan A 2005 *J. Appl. Phys.* **98** 054911
- [55] Maeda K, Sato M, Niikura I and Fukuda T 2005 *Semicond. Sci. Technol.* **20** S49–54

- [56] Ntep J M, Said H S, Lusson A, Tromson-Carli A, Ballutaud D, Didier G and Triboulet R 1994 *J. Cryst. Growth* **207** 30–4
- [57] Nause J and Nemeth B 2005 *Semicond. Sci. Technol.* **20** S45
- [58] Zhang D H and Brodie D E 1995 *Thin Solid Films* **261** 334
- [59] Dhar S, Pugel D, Hullavarad S S, Vispute R D, Ogale S B and Venkatesan T 2006 Investigation of thermally induced disorder and its recovery in ZnO single crystals by elastic resonant ion channeling *Proc. 13th World Oxide Electronics Workshop (Ischia, Italy)* PII-12 p 159 [http://www.woe13.it/abstract\\_book.pdf](http://www.woe13.it/abstract_book.pdf)
- [60] Chevtchenko S A, Moore J C, Ozgur U, Gu X, Baski A A and Morkoc H 2006 *Appl. Phys. Lett.* **89** 182111
- [61] 1982–1983 *CRC Materials Science and Engineering Handbook* 63rd edn
- [62] Vispute R D, Hullavarad S S, Pugel D E, Kulkarni V N, Dhar S, Takeuchi I and Venkatesan T 2005 Wide band Gap ZnO and ZnMgO heterostructures for future optoelectronic devices *Thin Films and Heterostructures for Oxide Electronics* ed S Ogale (Berlin: Springer)